CHAPTER 3

Synthesis of highly fluorescent nitrogen-rich carbon quantum dots and their application for the turn-off detection of cobalt (II)

3.1. Introduction

Vitamin B-12 is a water-soluble complex which contains essential element cobalt. It plays an important role as a cofactor in various enzymatic reactions such as the formation of methyl malonic acid, synthesis of methionine, and metabolism of purine and folates [Lison (1996)]. It also plays a crucial role in the functioning of the human body mainly in the nourishment of red blood cells (RBC's) and the preservation of nerve cells. Vitamin B-12 deficiency can lead to the development of severe neurologic damage and life-threatening pernicious anemia, i.e., vitamin B-12 anemia [Zhang *et al.* (2013)]. Its insufficiency can also cause symptoms of psychosis and mania [Zhang *et al.* (2013)]. However, excessive amount causes asthma, rhinitis, and cardiomyopathy [Barceloux & Barceloux (1999)]. Therefore, it has become an urgent need for the rapid, reliable, non-costly, and selective detection of Co^{2+}.

Various spectroscopic methods have been established for the quantitative evaluation of Co^{2+} including Atomic Absorption Spectrophotometry, Inductively Coupled Plasma Mass Spectroscopy, Auger Electron Spectroscopy, absorption, and chemiluminescence [Contino *et al.* (2016), Zhang *et al.* (2012), Sakamoto-Arnold *et al.* (1987), Yao *et al.* (2010), Mehta *et al.* (2013)]. The above proposed methods are very sensitive and selective but the need of sophisticated instrumentations, expertise and time consumption limited their ideality in real-time detection of Co^{2+} in environmental samples [Contino *et al.* (2016)]. Hence, to overcome these difficulties, it is necessary to develop a convenient, manageable, and cost-effective technique for environmental safety and health purpose. The fluorescence-based assay has been established as an unconventional technique to detect Co^{2+} which has several benefits such as non-costly, high sensitivity, less cell-damaging and fast response time.

The metal-based semiconductor fluorescent quantum dots such as CdTe and organic fluorescent dyes have established much attention for their unique optical properties and tremendous application in sensing, imaging, and optronic devices [Dong *et al.* (2012), Chan *et al.* (1998). Zi *et al*. fabricated the thioglycolic acid-capped $CuInS_2$/ZnS quantum dots for the Co^{2+} detection [Zi *et al.* (2014)], Zhong *et al*. prepared the different sized Cd-Te quantum dots for the Co^{2+} detection [Zhong *et al.* (2009)], and Bian *et al*. designed the Mn-doped ZnS quantum dots probe towards the Co^{2+}detection [Bian *et al.* (2014)]. However, in these methods, the use of heavy metal and organic solvents limits their ideality for their well-known toxicity and environmental distress. Thus, it is necessary to build up the non-toxic route towards the production of fluorescent materials.

Recently, carbon-based quantum dots (CQDs) is a worthy substitute over the traditional semiconductor quantum dots in aspects of the photoluminescent properties, biocompatibility, low-cytotoxicity, excellent water solubility, ease of functionalization, and offers the very high emission quantum yield [Zhou *et al.* (2012), Gong *et al.* (2015), Rosi *et al.* (2005)]. So these materials are potentially stabilized for the chem/biosensors, imaging, and diagnosis applications [Prasannan *et al.* (2013), Zhu *et al.* (2015), Wang *et al.* (2016)]. Various methodologies are involved for the synthesis of CQDs counting laser ablation, hot injection method, electrochemical oxidation, hydrothermal, and microwave assisted pyrolysis [Zhai *et al.* (2012), Tian *et al.* (2009), Zhu *et al.* (2009)]. However, the laser ablation requires the use of sophisticated and costly instrument, electrochemical oxidation necessitate highly concentrated acid which restricts their applicability, microwave irradiation offers easy pathway within a few minutes, but the unmanageable reaction condition limited its utility

[Bano *et al.*. (2018)]. Consequently, the hydrothermal route is generally preferred as it is simple, rapid, controllable, and cost-effective [Bano *et al.* (2018), Alam *et al.* (2015)].

Herein, nitrogen-rich CQDs (N–CQDs) have been prepared using a low-cost glycine as a carbon and nitrogen precursor and polyethyleneimine (PEI) is used as nitrogen doping as well as a surface passivating agent by a simple one-step hydrothermal treatment. The prepared N–CQDs exhibited the strong blue fluorescence at the excitation wavelength of 365 nm under UV light. Moreover, the as-prepared N–CQDs demonstrated very high QY up to 57% using quinine sulfate as a reference. By using these N–CQDs, very selective and sensitive approach is developed for the detection of Co^{2+} via quenching mechanism.

3.2. Materials and method

3.2.1. Synthesis of N–CQDs

Typically, 1 g of glycine and 0.6 g of PEI were taken and poured into a 15 mL of ultrapure water in a small beaker. The obtained solution was ultrasonicated for 15 min to get dispersion. Furthermore, the reaction mixture was transferred into a 15 mL of Teflon-lined autoclaved and heated at the temperature of 200 ºC for 4 hours. After that, the reaction mixture was cooled down to room temperature (RT). The appearance of the brown color of the reaction mixture was indicated the formation of N–CQDs. The obtained solution was centrifuged at 10,000 rpm up to 15 min to remove the foreign particles. Finally, the filtrate part was purified against the dialysis membrane for 2 days to obtain pure N–CQDs.

3.2.2. Experimental methodology

The as-prepared N–CQDs were characterized through various analytical techniques. The optical properties were conducted by UV-visible Spectrophotometer (Evolution 301, Thermo Scientific) and Fluorescence Spectrophotometer (Varian CaryEclipse). The shape and size were recorded on the Transmission Electron Microscope (TEM, TECHNAI G^2 20 S–TWIN). The Elemental investigation was carried out by the Energy Dispersive X-ray Spectroscopy (EDAX) equipped with TEM. Zeta potential was measured by using Nano-Zetasizer (MALVERN Instruments). The crystalline nature was analyzed by the X-Ray Diffractometer (XRD) (Rigaku MiniFlex 600) having Cu Kα radiation source and Ni filter in the range of 10–70° at a scanning rate of 5° min^{-1}. The various functional groups were investigated by using Fourier Transform Infrared Spectrophotometer (FTIR, Perkin Elmer Spectrum 100). The chemical composition, surface state and bonding present on the surface were probed by the X-Ray Photoelectron Spectroscopy (XPS, AMICUS, Kratos Analytical, A Shimadzu). The fluorescence decay measurement was conducted by Edinburgh Instrument, using a laser of wavelength 375.8 nm with pulse width 73.5 ps.

3.2.3. Quantum yield determination

The quantum yield of the N–CQDs was measured in reference to quinine sulphate from the given **equation 2.3** mentioned in **chapter 2** in a **section 2.6.1.**

3.2.4. Stern-Volmer quenching constant calculation

The Stern-Volmer quenching constant was calculated by the **equation 2.5** given in **chapter 2** in a **section 2.6.3**.

3.2.5. Detection of Co^{2+}

The turn-off detection of Co^{2+} was performed at RT in a HEPES buffer (0.2 M, pH 8). In a typical assay, 50 µL of the as-prepared N–CQDs was maintained in a 1 mL of HEPES buffer and then added the calculated amount of the Co^{2+} solution. The FL emission spectra of the reaction were traced after 10 min of incubation at 360 nm excitation. Additionally, the detection limit (LOD) was measured from the following equation along with the signal to noise ratio 3 (S/N=3) from the **equation 2.4** given in **chapter 2** (**section 2.6.2**).

3.3. Results and discussion

3.3.1. Characterization of N–CQDs

The N–CQDs were synthesized by a simple one-step hydrothermal treatment of glycine and PEI for 4 hours at 200 °C (**Scheme 3.1**). The formation of the N–CQDs was probed by various microscopic and spectroscopic techniques.

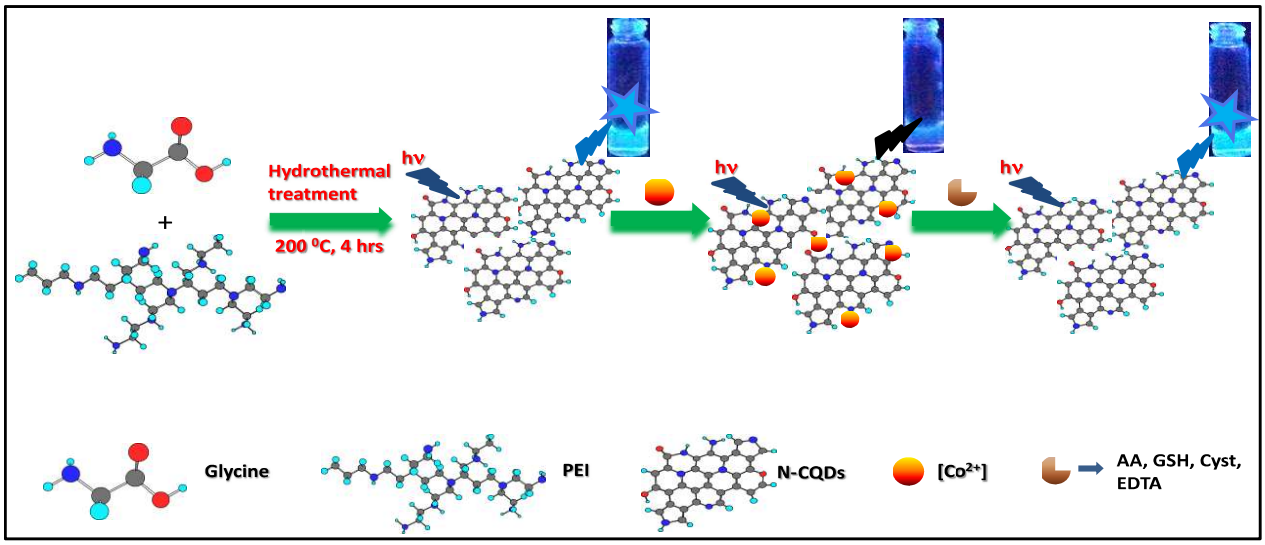

Scheme 3.1 Illustration of the one-step hydrothermal synthesis of N–CQDs and its application towards the detection of Co^{2+}.

The TEM micrograph explored the abundance of spherical and well dispersed N–CQDs **(Figure 3.1a)**. The broad circular ring in the SAED micrograph established that the as-prepared N–CQDs are amorphous, as shown in inset **Figure 3.1a**. The **Figure 3.1b** showed the particle size measurement histogram of the as-prepared N-CQDs which represented that the maximum particles are in the range of 2 to 2.5 nm. The amorphous nature of the as-prepared N–CQDs is identified by the XRD analysis **(Figure 3.1c)**. The broad reflection at 2θ=23° resembled the (002) plane of graphite, suggested the amorphous nature of as-prepared N–CQDs, which is consistent with the earlier reported literature [Lin *et al.* (2015), Hsu *et al.* (2012)]. The FTIR analysis revealed the attach functional groups on the N–CQDs surface (**Figure 3.1d)**. The peak at 3427 cm^{-1} is assigned to the –OH/–NH stretching mode of vibration. The peaks at 2928 cm^{-1} and 2851 cm^{-1} are due to the $–CH_x$ stretching modes of vibrations. The peaks in between the 1269 cm^{-1} and 1659 cm^{-1} are attributed to the O=CNH– stretching vibration in an aromatic heterocyclic ring; which confirmed the graphitic structures of the as-prepared N–CQDs [Dong *et al.* (2012), Yu *et al.* (2016), Liu *et al.* (2012].

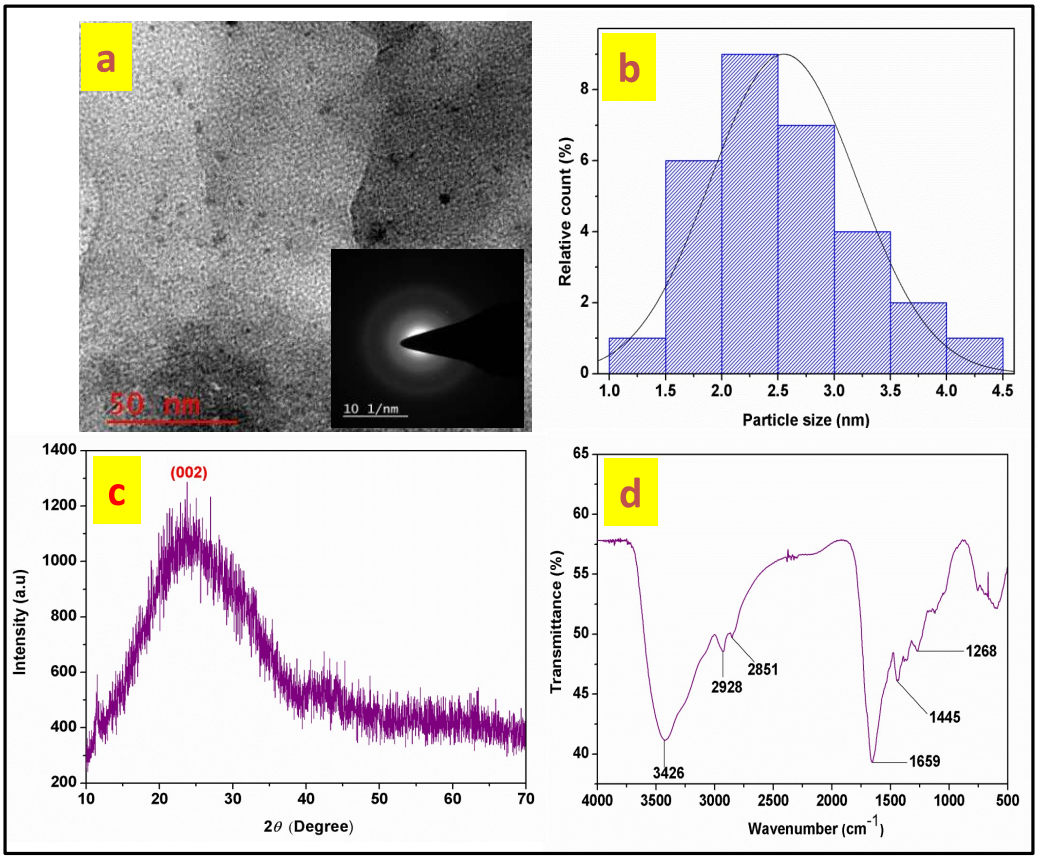

Figure 3.1 (a) TEM micrograph of N–CQDs whereas inset shows the SAED micrographs of N–CQDs, (b) particle size histogram, (c) XRD spectrum of N–CQDs at scan rate 5°/min in a range 10–70°, (d) FTIR spectrum of the as-prepared N–CQDs in a range 500–4000 cm^{-1}.

The EDAX analysis explored the presence of strong spectral signals of carbon (58.68%), oxygen (18.92%), and nitrogen (22.40%) which advocated the good doping of nitrogen into the N–CQDs matrix (**Figure 3.2)**. Further, the chemical composition, surface state, and bonding within the N–CQDs were probed by the XPS analysis. As shown in **Figure 3.3a,** the full range XPS spectrum exhibited the binding energies of C 1s, O 1s, and N 1s at 286.5 eV, 401 eV, and 533 eV, respectively. This result confirmed that carbon,

nitrogen, and oxygen are the main elements of the as-prepared N–CQDs [Qu *et al.* (2013), Tang *et al.* (2012), Li *et al.* (2015)]. Furthermore, the C1s spectrum of the N–CQDs showed the peaks at 284.9 eV (C=C), 285.8 eV (C=N), 286.5 eV (C–OH), 287.1 eV (C=O), and 287.8 eV (O=C–N–), as shown in **Figure 3.3b** [Zhou *et al.* (2015)]. The close look of the O 1s spectrum represents the peak at 532.5 eV (–OH/C–O–C) and 533.8 eV (C=O), as shown in **Figure 3.3c** [Zhang *et al.* (2012)]. Moreover, the N 1s spectrum of N–CQDs corroborated the presence of three peaks at around 399.5 eV (C–N–C), 400.7 eV (N–H), and 402.3 eV ($N–C_3$), as shown in **Figure 3.3d** [Lin *et al.* (2015), Liu *et al.* (2012), Tang *et al.* (2013)]. This result supports the FTIR analysis which revealed the occurrence of amino, hydroxyl, and carbonyl functional moieties on the N–CQDs surface.

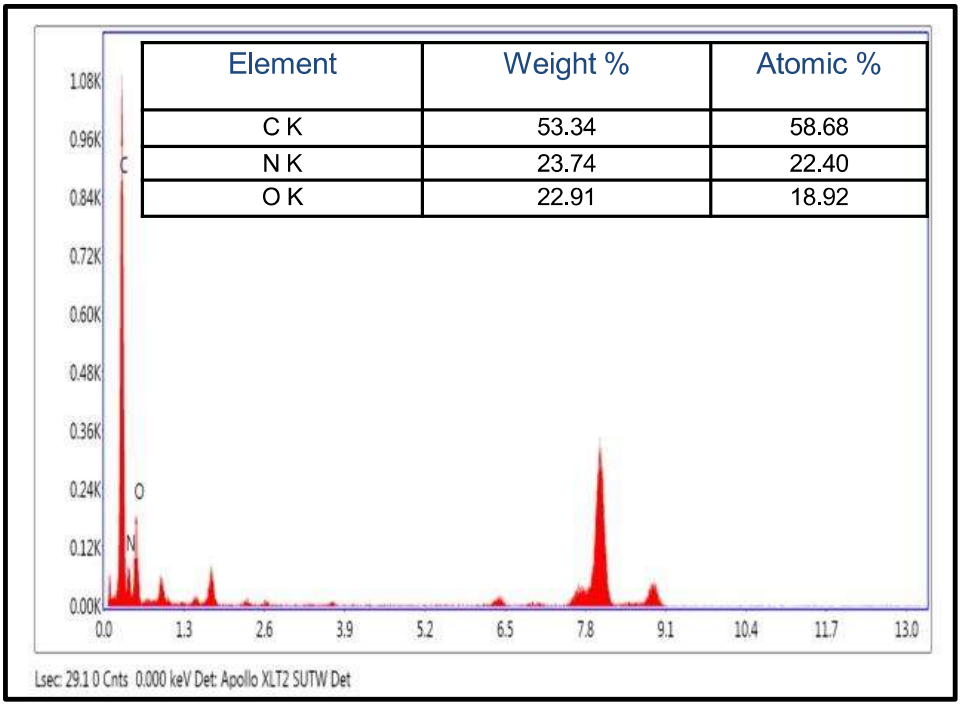

Figure 3.2 EDAX analysis of the as-prepared N-CQDs composed of C, O and N, inset shows the elemental composition.

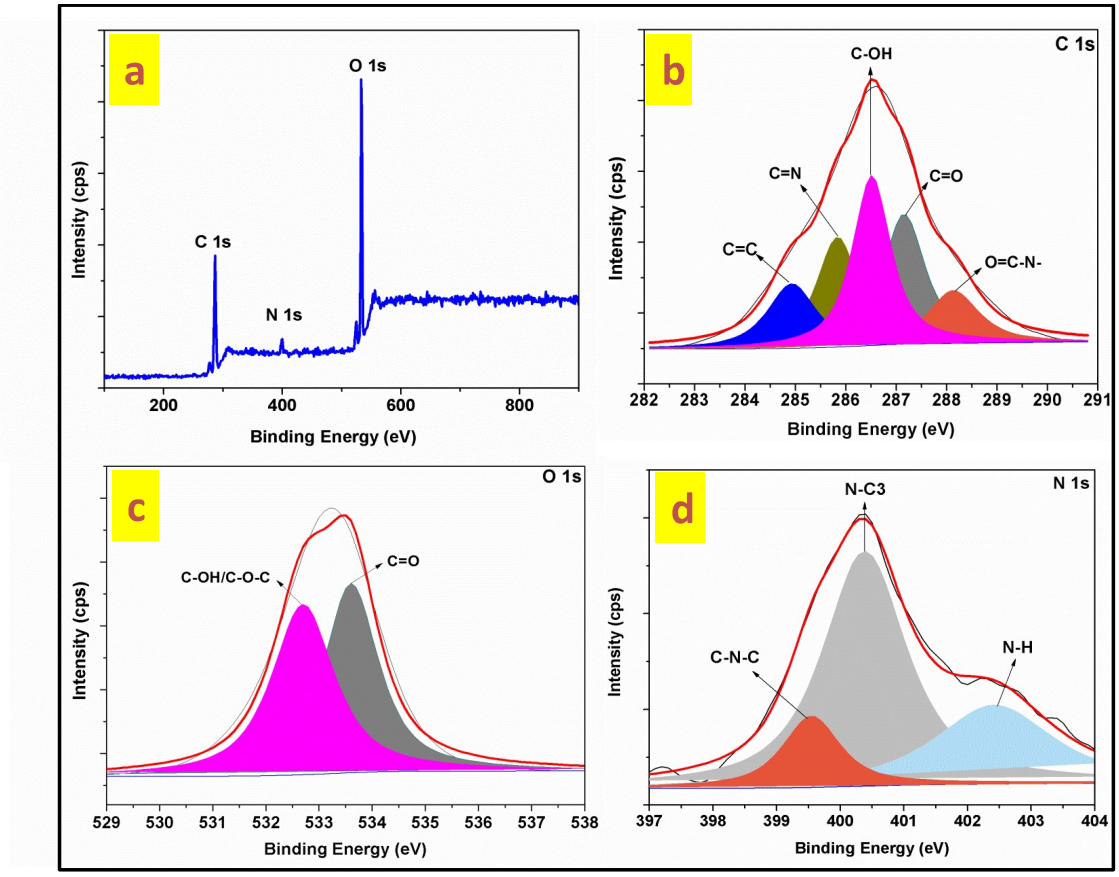

Figure 3.3 Correspond to the (a) Wide scan spectrum, (b) C 1s spectra, (c) O 1s spectra, (d) N 1s spectra of the N-CQDs.

3.3.2. Optical properties of the N–CQDs

The optical properties of the prepared N-CQDs were also investigated for the future application in biological and analytical diagnostics. As indicated in **Figure 3.4a,** black line presents the UV-visible absorbance while the blue line shows a fluorescence emission spectrum of the as-prepared N–CQDs**.** The UV-visible spectrum exhibited a single absorbance band at 336 nm which is due to the n-π* transition of C=N/C=O and fluorescence emission spectrum is centered at 464 nm [Qu *et al.* (2013)]. As represented in inset **Figure**

3.4a, the as-prepared N–CQDs exhibited a strong blue emission under the excitation of 365 nm in a UV chamber; this confirmed the fluorescent nature of the as-prepared N-CQDs. The pure blue color fluorescent emission of as-prepared N–CQDs is further confirmed by the Commission International De L'Eclairage (CIE) co-ordinates at (0.14, 0.15) which is obtained from the fluorescence emission data, as shown in **Figure 3.4b**. Furthermore, the N-CQDs exhibited the excitation-dependent emission ranged from 280 to 400 nm, as indicated in **Figure 3.4c**. This result demonstrated that the N-CQDs might have the various trapped surface for the emission. It was found that the addition of different concentration of NaCl (0–100 mM) unchanged the FL emission intensity of N-CQDs (**Figure 3.4d)**. This result indicated that the as-prepared N–CQDs did not aggregate and stable even under high ionic strength atmosphere.

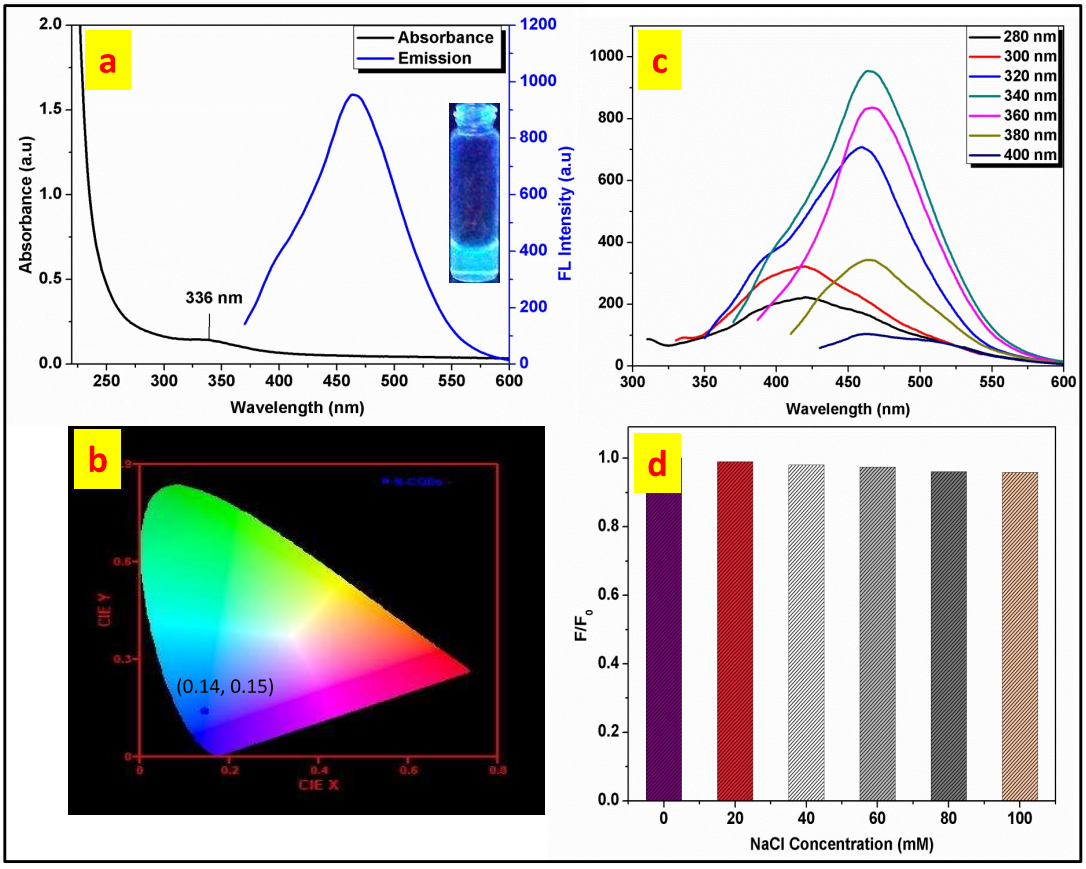

Figure 3.4 (a) UV-visible spectrum (black) and FL emission intensity (blue) at the excitation wavelength of 360 nm of N-CQDs, (b) CIE co-ordinates for the blue FL emission of N-CQDs, (c) represents the FL emission intensity at the different excitation wavelength (280–400 nm), (d) showing the stability under high ionic strength after the addition of different NaCl concentration (0–100 mM)

Apart from this, the emission intensity of the N–CQDs not showed any precipitation and photo-bleaching effect of the particles even after 6 months of incubation at 4 ^{o}C (**Figure 3.5)**. This result confirmed that the as-prepared N–CQDs are highly stable at ambient conditions. Such a highly stable N-CQDs have much potential for sensing and other analytical applications. However, the mechanism of strong fluorescence is still debatable [Zhang & Chen (2014)].

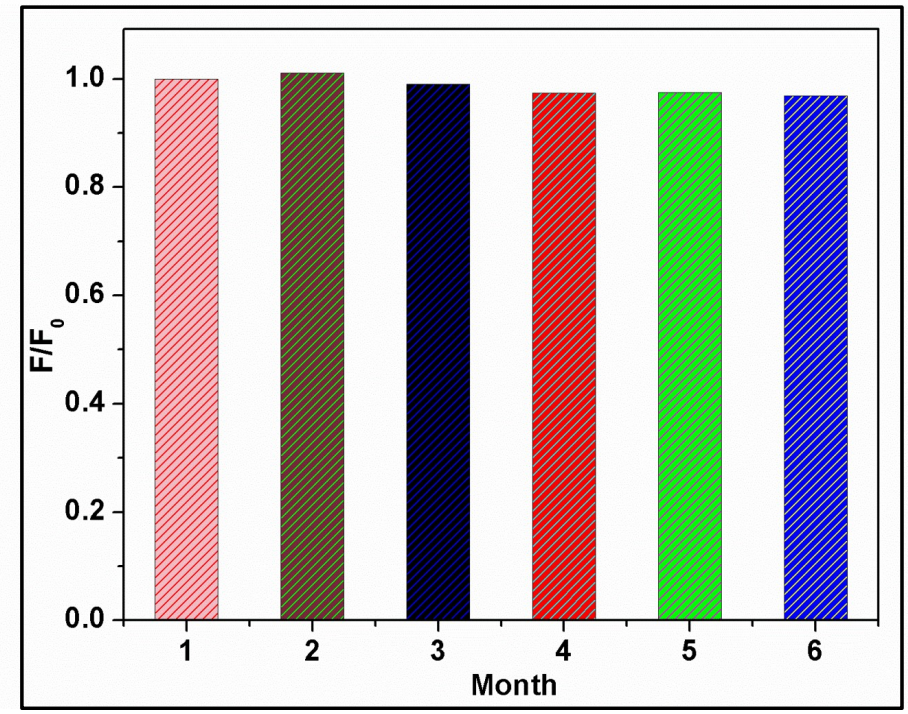

Figure 3.5 Stability of N–CQDs at ambient temperature, FL emission intensity remains unchanged even after 6 month of incubation.

In previous studies, it is given that blue fluorescence is due to the band gap arises from the localization of electron-hole pairs in nano-sized sp^2 hybridized domains which are present in a carbon-oxygen sp^3 matrix [Bano *et al.* (2018), Eda *et al.* (2010)]. Thus, the doping with strong electron withdrawing nitrogen atoms and the presence of hydroxyl moieties make a significant part to yield a blue fluorescence emission in the synthesized N-CQDs. The calculated QY of the prepared N-CQDs is 57% at 360 nm excitation using quinine sulfate as a reference (QY = 54% in a 0.1 M H_2SO_4). It is also observed that the prepared N-CQDs have very high QY as compare to the earlier reported literature [Dong *et al.* (2012), Yu *et al.* (2016), Li *et al.* (2015), Lu *et al.* (2012), Edison *et al.* (2016) Kong *et al.* (2016)]. The high QY of the N-CQDs is accounted by the FTIR, EDAX, and XPS analysis

which elaborated the surface passivation of N–CQDs with –OH, –C=O, O=C–NH functional groups. The presence of nitrogen and oxygen-rich functional groups could effectively enhance the intrinsic state emission by reducing the non-radiative recombination of electron-hole pairs resulting to the increase in QY. Thus, the prepared N-CQDs could offer great potential in biological and analytical applications.

3.3.3. Detection Assay

3.3.3.1. Effect of pH

The pH effect was also studied carefully toward the detection of Co^{2+}. On changing the pH from 2 to 8, the emission intensity of the N–CQDs increased and prolonged to this; it decreased (**Figure 3.6a)**. This result illustrated the present sensing system is sensitive to the pH used. So the detection of Co^{2+} was also investigated under different pH ranged from 2 to 12. As shown in **Figure 3.6b,** it is observed that the sensing potential of N–CQDs varied with the pH value and maximum change in FL emission is obtained at pH 8. Thereafter, it is noticed that on further increasing the pH, the change in FL emission started to decrease. The reason behind this phenomenon is that in highly acidic media (< pH 8) amino groups present on the N–CQDs surface get highly protonated and thus unable to form complex with Co^{2+}. However, in highly alkaline media (> pH 8) the partial hydrolysis of Co^{2+} reduced the complex formation between the amine group of the N–CQDs and Co^{2+}.

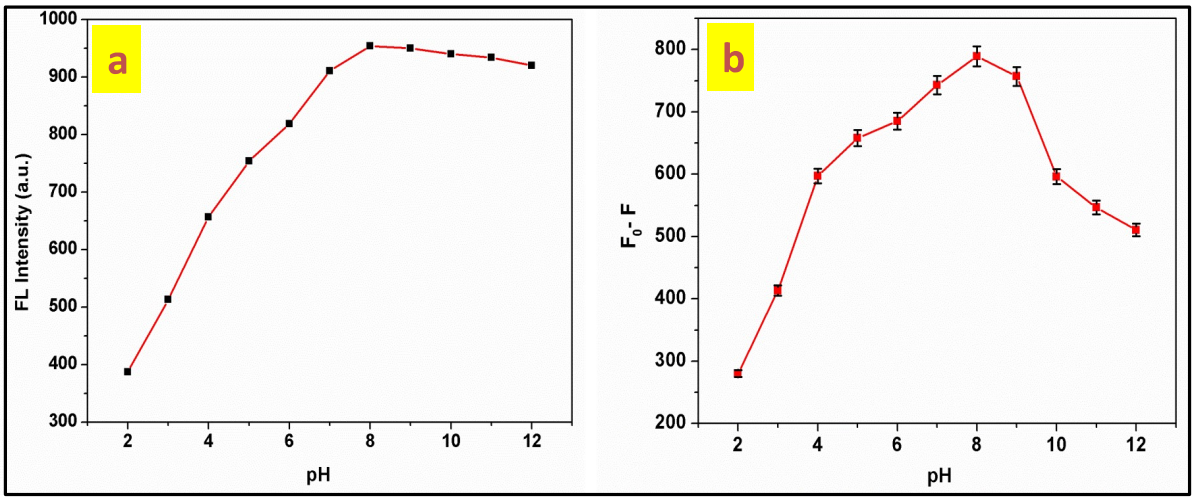

Figure 3.6 (a) FL emission intensity of N–CQDs at different pH range from 2 to 12, (b) emission intensity of N–CQDs towards the detection of Co^{2+} in different pH range from 2 to 12 (F_0 and F are the FL emission intensities of N–CQDs in the absence and presence of Co^{2+}, respectively). Error bar is showing the three replicate measurements.

3.3.3.2. Selectivity and sensitivity toward the detection of Co^{2+}

Selectivity is an essential factor to measure the sensing performance of the prepared N–CQDs. Hence, to explore the selectivity, 100 µL of the prepared N–CQDs was maintained in a 1 mL of HEPES buffer (0.2 M, pH 8). Thereafter, 100 µL of various metal ions, including Mn^{2+}, Al^{3+}, Cd^{2+}, Hg^{2+}, Zn^{2+}, Pb^{2+}, Co^{2+}, As^{3+}, Ca^{2+}, Mg^{2+}, Fe^{2+}, Fe^{3+}, Cu^{2+}, and Ni^{2+} ions (100 µM) was added into it and FL emission spectra were recorded individually. As indicated in **Figure 3.7**, the fluorescence quenching is observed after the addition of 100 µL of Co^{2+} (100 µM) while in the case of other metal ions only a slight change is observed as compared to blank and the effect is almost negligible. Inset **Figure 3.7** showed the photographs of vials in the presence of different metal ions under UV light. This result clearly indicated that the N–CQDs have high selectivity toward the detection of Co^{2+}.

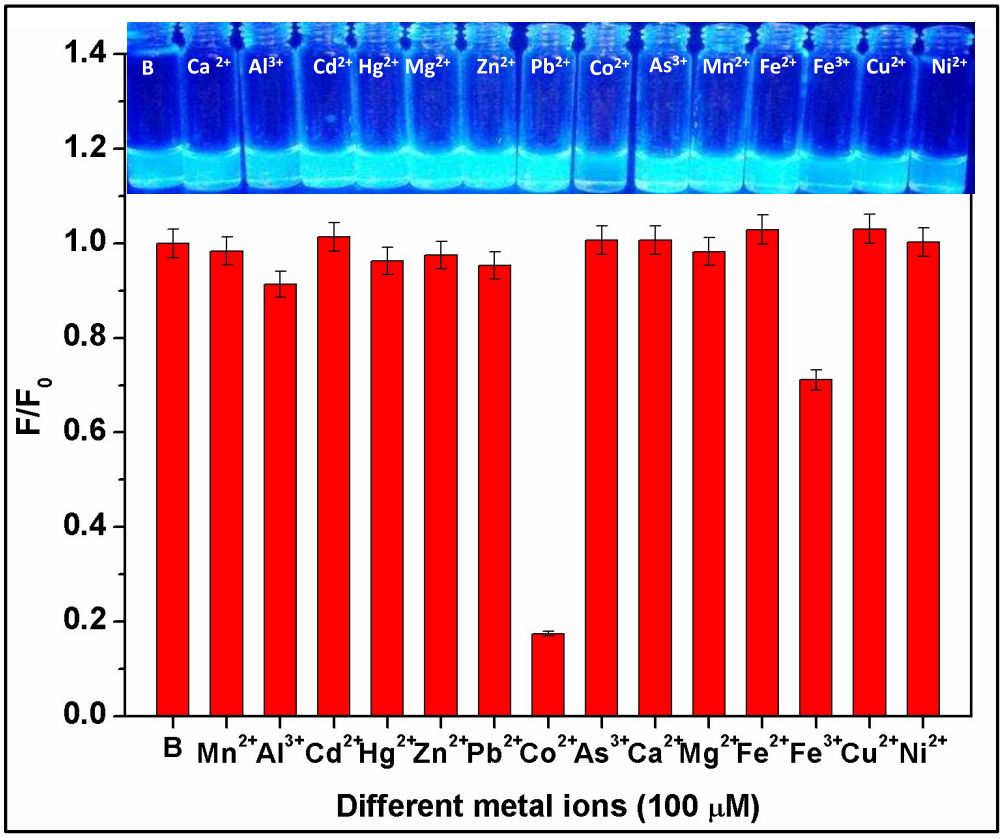

Figure 3.7 (a) Ratio between the fluorescence changes after the addition of various metal ions (100 μM) including (Mn^{2+}, Al^{3+}, Cd^{2+}, Hg^{2+}, Zn^{2+}, Pb^{2+}, Co^{2+}, As^{3+}, Ca^{2+}, Mg^{2+}, Fe^{2+}, Fe^{3+}, Cu^{2+}, and Ni^{2+}) in a prepared N–CQDs whereas inset shows the photographs of vial after the addition of different metal ions in a UV light.

The competitive study for the detection of Co^{2+} was also studied carefully in a mixture of different interfering metal ions including Mn^{2+}, Al^{3+}, Cd^{2+}, Hg^{2+}, Zn^{2+}, Pb^{2+}, As^{3+}, Ca^{2+}, Mg^{2+}, Fe^{2+}, Fe^{3+}, Cu^{2+}, and Ni^{2+} (100 μM). The addition of 100 μL of Co^{2+} (100 μM) salts in a mixture effectively quenched the emission of the N–CQDs, as shown in **Figure 3.7**. This observation confirmed that the proposed method can still detect the Co^{2+} in a mixture.

Hence, it is proved that the prepared N–CQDs probe could offer a credible anti-interference ability toward Co^{2+} detection.

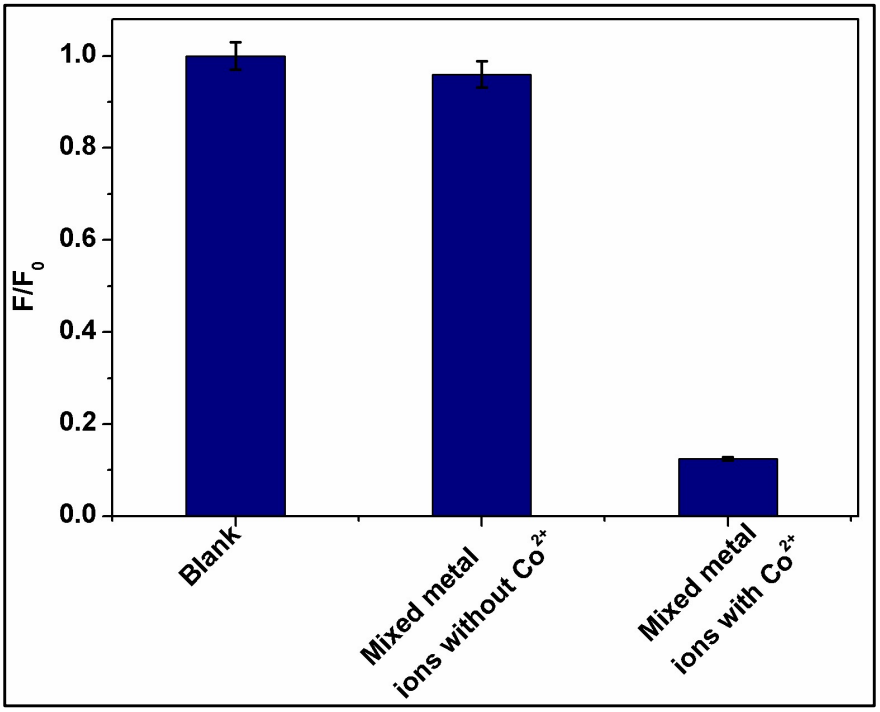

Figure 3.8 Sensitivity of the Co^{2+} in a mixture of different metals ions (100 μM), error bar shows the three independent measurement.

Beside the selectivity, sensitivity is also a significant parameter to assess the sensing performance of the proposed system. The FL emission of the N–CQDs at around 464 nm decreased gradually with the increase in Co^{2+} concentration (0–50 μM), as shown in **Figure 3.9a.** This result suggested that the present sensing system is highly sensitive towards the detection of Co^{2+}. As indicated in **Figure 3.9b**, the linear correlation graph is obtained between $F_0/F-1$ and Co^{2+} concentration with R^2=0.997 in a range of 0.5–3 μM. The calculated Stern-Volmer quenching constant in this experimental condition is found to be 0.046×10^6 $L.Mol^{-1}$. This result confirms that the as-prepared N–CQDs are highly sensitive

towards the detection of Co^{2+}. In the same experiment, the calculated detection limit for Co^{2+} detection is found to be 0.12 μM according to the equation S/N=3 which is much lower up to its maximum permissible limit (1.7×10^{-3} M) in drinking water recommends by World Health Organization (WHO) [Kim *et al.* (2006)]. It is also observed that the obtained detection limit is much lower as compared to another sensing probe reported in earlier literature, as displayed in **Table 3.1** [Zhang *et al.* (2012), Kong *et al.* (2016), Sung *et al.* (2013), Shi *et al.* (2013), Wen *et al.* (2016), Liu *et al.* (2017), Chen *et al.* (2017), Liao *et al.* (2018)].

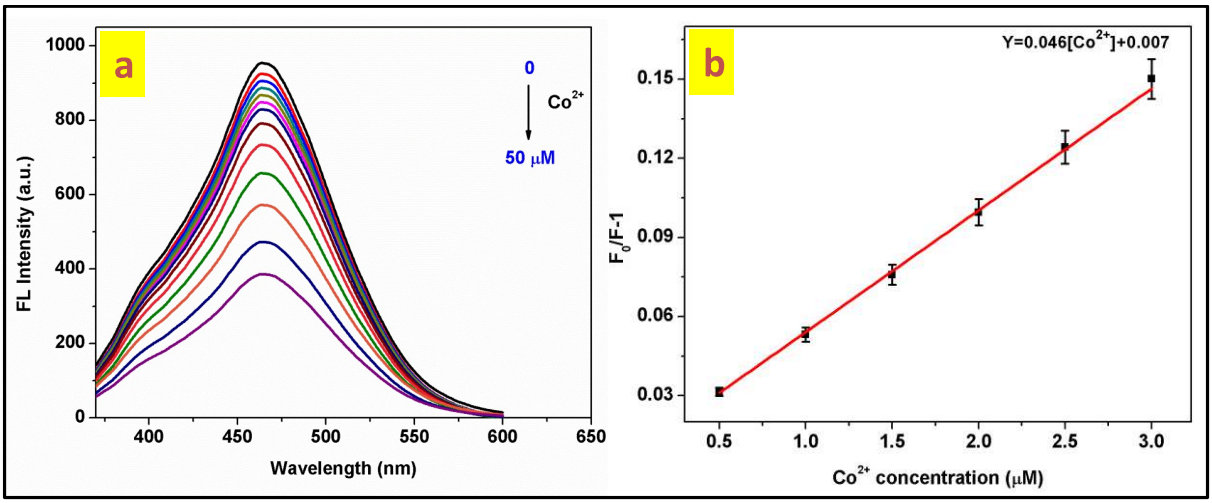

Figure 3.9 (a) Showing the FL emission spectra after the addition of different concentration of Co^{2+} (0–50 μM) in a N–CQDs, (b) reveals the plot between $F_0/F-1$ versus concentration of Co^{2+} and shows the linear correlation in a 0.5-3.0 μM range. Error bars demonstrates the standard deviation of the three replicate measurements.

Table 3.1. Comparison of proposed method with earlier reported literature toward the detection of Co^{2+}.

Detection Method	Probe	Detection limit	Linear range	Real Sample	Ref.
Absorbance	GSH–AgNPs	5 μM	5–400 μM	-	[Sung *et al.* (2013)]
Absorbance	P–AuNPs	2 μM	2–10 μM	-	[Zhang *et al.* (2012)]
Chemiluminescence	Polymer	0.67 nM	1–1000 nM	-	[Shi *et al.* (2013)]
Fluorescence	N–CDs	0.68 μM	1–100 μM	-	[Wen *et al.* (2016)]
Fluorescence	N–CDs	0.40 μM	1–90 μM	Vitamin B-12	[Liu *et al.* (2017)]
Fluorescence	N,S–CDs	80 nM	0.08–100 μM	River water	[Chen *et al.* (2017)]
Fluorescence	P,N–CQDs	0.053 μM	0–60 μM	River water	[Liao *et al.* (2018)]
Fluorescence	CDs	0.45 μM	0–40 μM	Lake and Tap water	[Kong *et al.* (2016)]
Fluorescence	N–CQDs	0.12 μM	0.5–3 μM	Vitamin B-12	[Bano *et al.* (2019)]

The fluorescence recovery of the quenched N–CQDs/Co^{2+} system was also investigated. It is observed that addition of ascorbic acid (AA), glutathione (GSH), cysteine (cyst), and ethylenediaminetetraacetic acid (EDTA) into the N–CQDs/Co^{2+} system solution recovered the fluorescence emission of quenched N–CQDs, as indicated in **Figure 3.10**. Thus, the prepared fluorescent N–CQDs can further act as a probe for the Co^{2+} detection. Hence, the prepared N–CQDs nano-probe provides the obvious advantages of effortlessness, convenience, and rapid performance toward Co^{2+} detection.

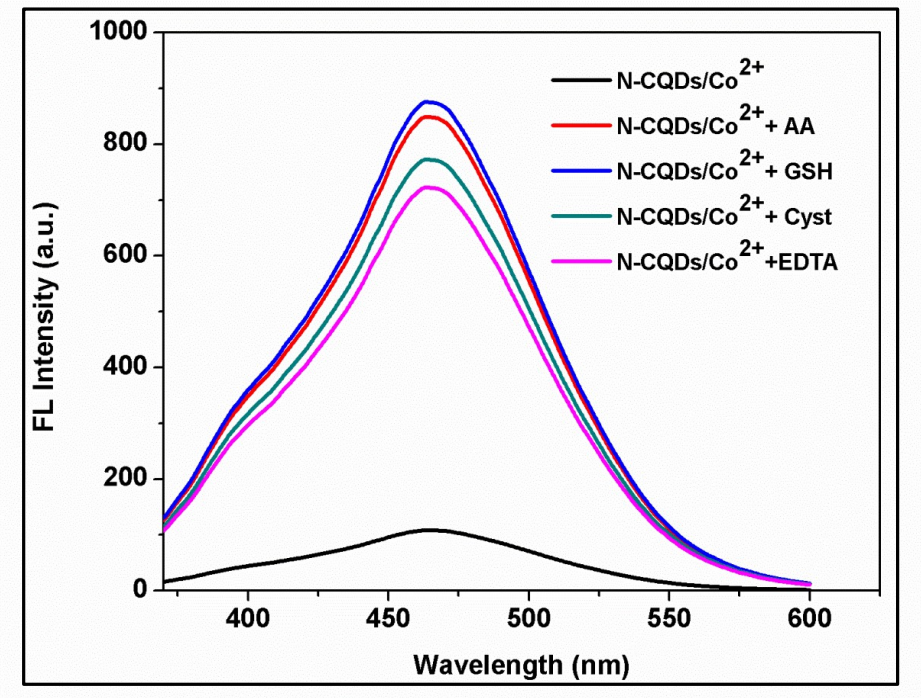

Figure 3.10 Fluorescence spectra after the addition of AA, GSH, EDTA, and cyst into the N–CQDs/Co^{2+} system ([AA]=[GSH]= [EDTA], and [Cyst]= 1 mM).

The mechanistic study of the proposed sensing system was also deliberated carefully. As shown in **Figure 3.10a**, the successfully overlapping of absorbance of Co^{2+} and emission spectra of N–CQDs assured that the inner filter effect (IFE) occurred in a very systematic way. In order to get the complete quenching mechanism, time-resolved fluorescence data were obtained before and after incubating the Co^{2+}, as shown in **Figure 3.11b**. The calculated average life time of the N–CQDs and N–CQDs/Co^{2+} are found to be 3.57 ns and 3.53 ns, respectively. Negligible change in fluorescence lifetime suggested the static quenching of N–CQDs which may be due to the specific interaction between N–CQDs and quencher molecule [Singh *et al.* (2018)]. Again N–CQDs/Co^{2+} reaction system was characterized through a TEM analysis.

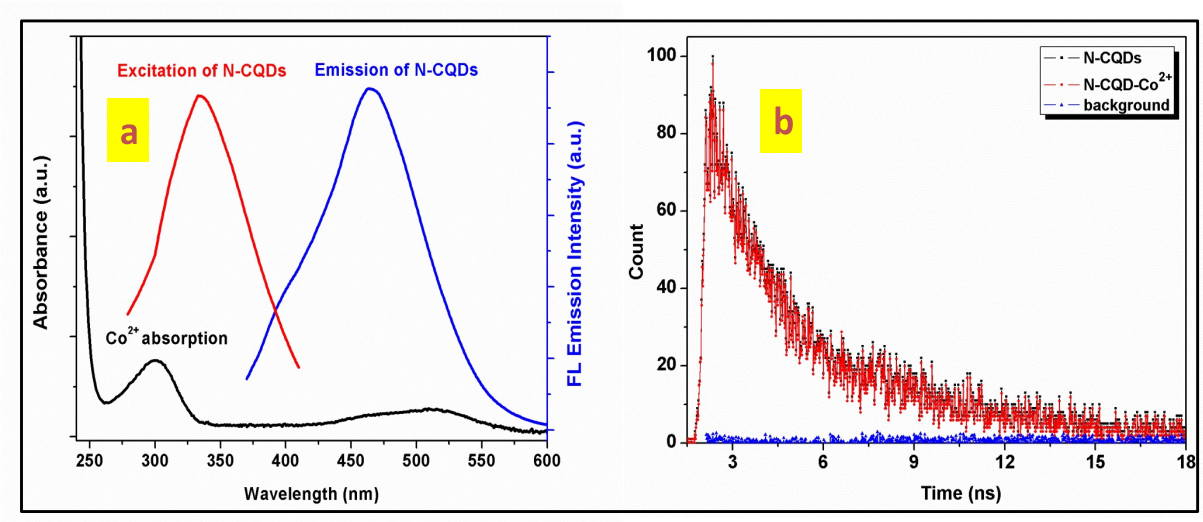

Figure 3.11 (a) Shows the overlapping of absorbance spectrum of Co^{2+} with excitation and emission spectrum of N–CQDs, (b) fluorescence decay spectra of N–CQDs before and after incubating of Co^{2+}.

As shown in **Figure 3.12**, it is confirmed that aggregation of N–CQDs seriously occurred in the presence of 100 µL of Co^{2+} (100 µM). It is also found that the addition of Co^{2+} in N–CQDs solution changes the solution color from light yellow to pale yellow (**Figure 3.13)**. This color change indicated the complex formation between the amino group of N–CQDs and Co^{2+} [Liu *et al.* (2017)].

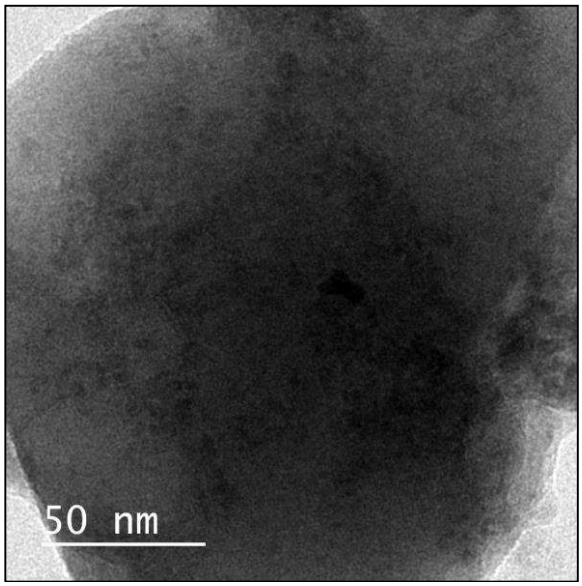

Figure 3.12 TEM micrograph of N–CQDs in the presence of 100 μL of Co^{2+} (100 μM).

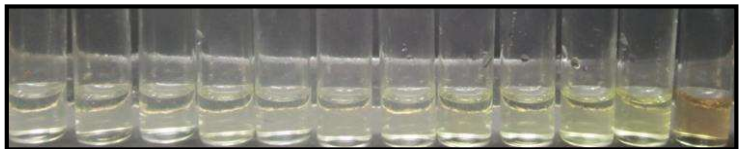

Figure 3.13 Corresponding color change of N–CQDs from transparent to pale yellow after the addition of Co^{2+} (0–100 μM).

To explore the complexation, the zeta potential of the N–CQDs was also measured before and after incubating the Co^{2+}. The zeta potential of the N–CQDs decreased from 19.5 to 15.5 mV respectively which elaborated that the Co^{2+} can adhere on the N–CQDs surface (**Figure 3.14**). Therefore, the quenching of N–CQDs may be assigned to the IFE, static quenching, aggregation, and formation of the cobalt-amine complex between the N–CQDs and Co^{2+}.

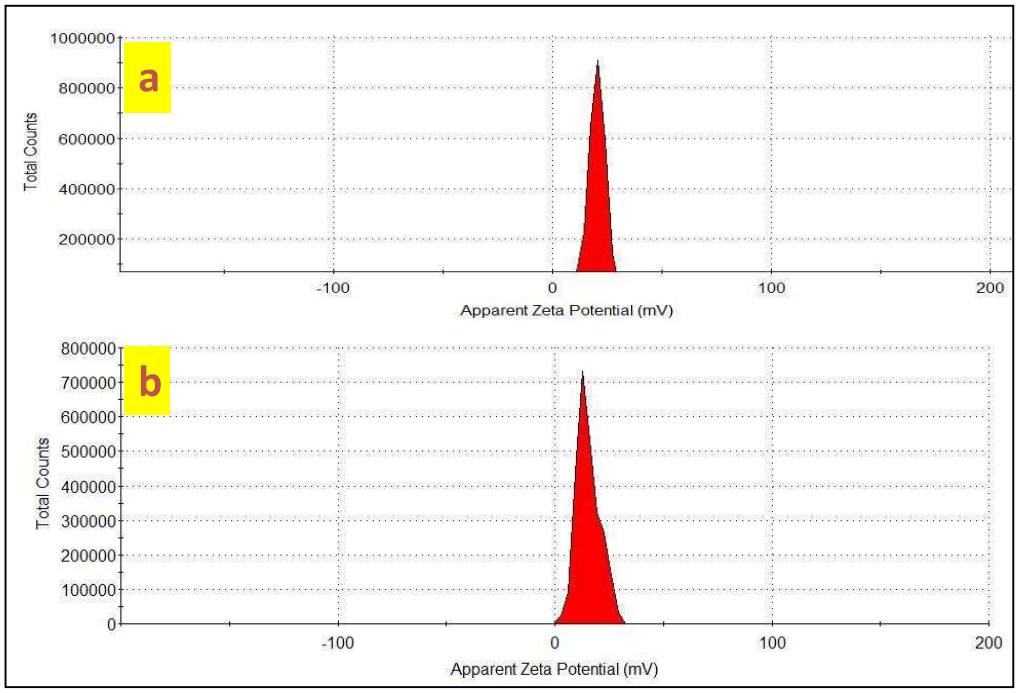

Figure 3.14 (a) DLS scan of N–CQDs and (b) N–CQDs/Co^{2+} system.

3.3.4. Detection of Co^{2+} in vitamin B-12 sample

In order to exploit the feasibility of the Co^{2+} probe system, standard addition method was performed with the vitamin B-12 injection sample. Vitamin B-12 injection was purchased from the local pharmacy of Varanasi, U.P., India. The collected sample was diluted 5-folds with ultrapure water. Further, the dilute vitamin B-12 sample was analyzed after spiking with the standard concentration of Co^{2+} (4, 8, and 12 μM) and recovery experiments were performed. It is noticed that the obtained values are reliable with the concentration of Co^{2+} added, as demonstrated in **Table 3.2.**

Table 3.2 Standard recovery test of spiked Co^{2+} in vitamin B-12 sample measured with N–CQDs.

Sample	Spiking (μM)	Found (μM)	Recovery (%)	RSD (%, n=3)
Vitamin B-12	0	12.6	-	1.63
	4	17.2	104.7	1.77
	8	21.3	105.5	1.34
	12	24.1	96.0	2.54

The found recoveries are in the range of 96.0–104.7 % and relative standard deviation (RSD) for three independent measurements is lower than 5% which is acceptable compared to that of other reported literatures [Jing *et al.* (2019), Zhao *et al.* (2019)]. Thus, our proposed method is tolerable and viable toward the trace level detection of Co^{2+} in a real sample analysis.

3.4. Conclusion

In this work, we have successfully prepared the highly fluorescent N–CQDs with high QY of 57% by using simple one-step hydrothermal treatment. The prepared N–CQDs are found to be a good nano-probe for the selective and sensitive detection of Co^{2+} with a detection limit of 0.12 μM in a linear range from 0.5 to 3.0 μM. The sensitivity of the detection system is achieved by the quenching mechanism based on the IFE, static quenching, aggregation, and formation of cobalt-amine complex amid the N–CQDs and Co^{2+}. The present sensing system is also successfully applied to the vitamin B–12 sample as the practical application of Co^{2+} detection. We hope that the present work may offer a new move towards the Co^{2+} detection along with other toxic ions having low cost, high sensitivity, and selectivity for the environmental, clinical, and analytical applications.